J. Phys.: Condens. Matter **11** (1999) 687–701. Printed in the UK PII: S0953-8984(99)96021-6

Study of $RFe_{12-x}Mo_x$ (R = Y, Ho) compounds by neutron powder diffraction, ac susceptibility and magnetization

J Ayres de Campos†, L P Ferreira‡, M M Cruz§, J M Gil‡, P J Mendes‡, I C Ferreira†, M Bacmann‖, J-L Soubeyroux‖, D Fruchart‖, M Godinho§ and N Ayres de Campos‡

† Departamento de Física, Universidade do Minho, P-4719 Braga, Portugal
‡ Departamento de Física, Universidade de Coimbra, P-3000 Coimbra, Portugal
§ Departamento de Física, FCUL, Campo Grande, P-1700 Lisboa, Portugal
‖ Laboratoire de Cristallographie du CNRS, BP 166, F-38042 Grenoble Cédex 9, France

Received 17 July 1998, in final form 26 October 1998

Abstract. Neutron powder diffraction, magnetization and ac susceptibility measurements were performed on compounds of the series $RFe_{12-x}Mo_x$ (R = Y and Ho, $x = 1, 2, 3$). The influence of the Mo content on both structural and magnetic properties is discussed. Comparison with published data for different Mo concentrations is made. It is found that the effect of Mo substitution for Fe on structural and magnetic properties can be described by two regimes separated by a critical Mo content around $x = 2$.

1. Introduction

The Fe-rich ternary compounds $RFe_{12-x}M_x$ (R = rare earth and M = Ti, V, Cr, Mo, Si) show interesting magnetic characteristics for possible permanent magnet applications [1]. These compounds crystallize in the tetragonal $ThMn_{12}$-type structure with space group $I4/mmm$ [2]. The third element M, which is necessary to stabilize the RFe_{12} structure, has a strong effect on the magnetic properties, leading to a reduction of the Curie temperature and magnetization.

The R atoms occupy the crystallographic 2a site and the Fe atoms occupy 8i, 8j and 8f sites. The Mo atom replaces Fe preferentially at the 8i sites [3, 4].

In this work, the structural and magnetic properties of $RFe_{12-x}Mo_x$ (R = Y, Ho; $x = 1$, 2 and 3) studied by neutron diffraction, ac susceptibility and magnetization are presented. A comparison with results by other authors for different Mo concentrations is made [5, 6]. The effect of Mo on the magnetic properties of the different sublattices is discussed.

2. Experimental details

The $RFe_{12-x}Mo_x$ (R = Y, Ho) compounds were prepared by melting the 4N-purity starting materials in a cold crucible induction furnace under 5N-purity argon atmosphere. In order to prevent an excessive evaporation of the low melting point element Y (Ho), the binary Fe–Mo composition was first prepared and then the third element was added. The samples were sealed in silica tubes filled with pure argon gas and annealed for 10 days at temperatures around 900 °C. The sample homogeneity was verified using conventional x-ray powder diffraction technique. The $ThMn_{12}$-type phase was found to be dominant, with small amounts of α-Fe present in some of the samples (always less than 4 wt%).

0953-8984/99/030687+15$19.50

Magnetic measurements were performed on non-oriented powder samples using a SQUID or VSM magnetometer, in the temperature range 5–400 K, under magnetic fields up to 10 T. Ho oriented powder samples with cylindrical shape were aligned in a field of 1 T and fixed with epoxy resin. For the ac magnetic susceptibility measurements a field with an amplitude of 10^{-4} T and a frequency of 95 Hz was used.

Neutron diffraction experiments were carried out at 6 K and 290 K at the Siloé reactor of the Centre d'Etudes Nucléaires and at the ILL D2B diffractometer, in Grenoble. A sample of $HoFe_{10.5}Mo_{1.5}$ was also measured at 290 K. The nuclear and magnetic structures were refined using the Rietveld method with the Fullprof program [7].

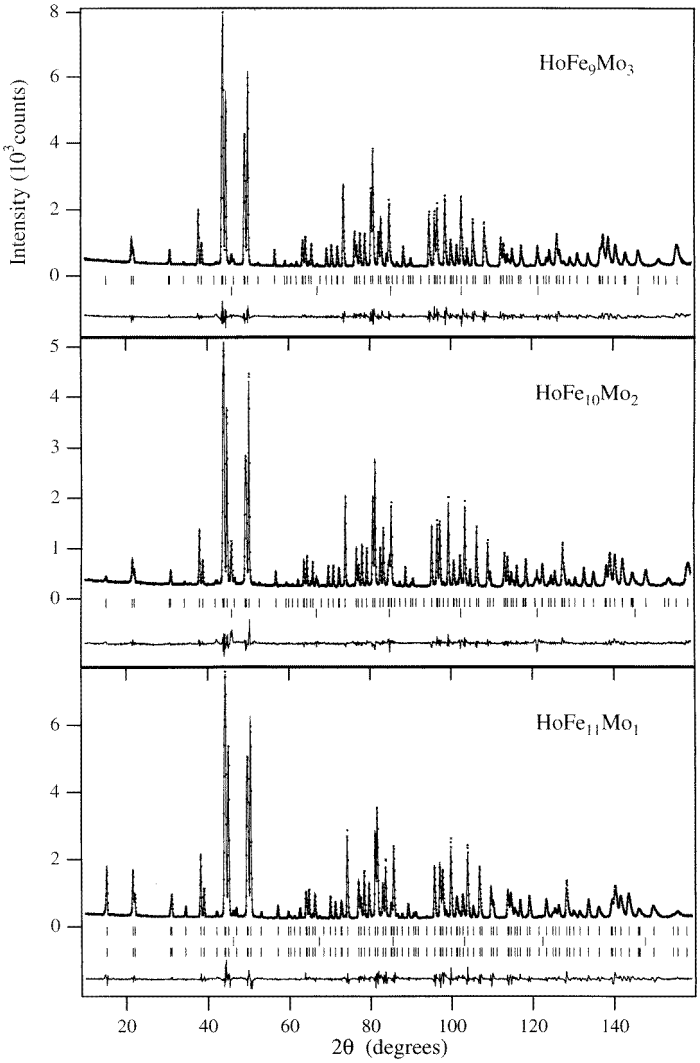

Figure 1. Experimental (dots) and calculated (lines) neutron diffraction diagrams for the Ho samples at 6 K. The difference pattern (observed − calculated) is shown in the bottom of each diagram. The short bars correspond to the nuclear peaks, the iron impurity and the magnetic peaks.

Table 1. Refined parameters and reliability factors from neutron diffractograms at room temperature: n is the Mo content/formula unit; x is the fractional position coordinate of 8i and 8j atoms; a and c are the lattice parameters; R_p is the profile factor and R_B is the Bragg factor.

	$YFe_{12-n}Mo_n$				$HoFe_{12-n}Mo_n$				
	$YFe_{11}Mo$	$YFe_{10}Mo_2$	$YFe_{9.5}Mo_{2.5}$ [10]	YFe_9Mo_3	$HoFe_{11}Mo$	$HoFe_{10.5}Mo_{1.5}$	$HoFe_{10}Mo_2$	$HoFe_{9.5}Mo_{2.5}$ [10]	$HoFe_9Mo_3$
n	1.07 (6)	2.22 (8)	2.40 (6)	2.98 (6)	1.15 (8)	1.71 (10)	2.38 (6)	2.50 (6)	2.90 (6)
x (8i)	0.3580 (3)	0.3578 (4)	0.3572 (3)	0.3573 (3)	0.3577 (3)	0.3579 (2)	0.3571 (1)	0.3577 (1)	0.3563 (2)
x (8j)	0.2769 (3)	0.2812 (4)	0.2823 (3)	0.2840 (3)	0.2784 (4)	0.2807 (1)	0.2816 (1)	0.2833 (1)	0.2847 (1)
a (Å)	8.515 (1)	8.554 (1)	8.561 (1)	8.595 (1)	8.499 (1)	8.521 (1)	8.536 (1)	8.559 (1)	8.576 (1)
c (Å)	4.783 (1)	4.802 (1)	4.808 (1)	4.832 (1)	4.779 (1)	4.784 (1)	4.795 (1)	4.807 (1)	4.824 (1)
R_p (%)	1.60	1.80	3.82	2.17	3.40	5.58	4.28	5.36	5.38
R_B (%)	3.81	4.48	3.75	3.79	2.45	3.84	4.90	4.49	3.66

3. Results and discussion

3.1. Crystal structure

Examples of the neutron diffraction patterns obtained for the Ho samples, together with the fitted profiles, are shown in figure 1. As expected, all patterns correspond to the tetragonal $ThMn_{12}$-type structure, space group $I4/mmm$, $Z = 2$, where Z is the number of formula units per cell. The refined structural parameters at room temperature for $RFe_{12-x}Mo_x$ are summarized in table 1. Good fitting results were obtained with Mo atoms occupying only 8i sites. Only minor differences were found between the nominal Mo content and the measured values.

Table 2 presents the average interatomic distances between each iron site and nearest neighbour iron atoms. Due to the different size of the Fe and Mo atoms (1.27 Å and 1.40 Å, respectively) a significant variation of the lattice parameters and interatomic distances with increasing Mo content was expected. However, this variation, although more perceptible in the ⟨Fe–Fe⟩ distances related to the 8i site, is not as marked as predicted [8].

Table 2. Average interatomic distances between each iron site and other iron nearest neighbours for (Y, Ho)$Fe_{12-x}Mo_x$.

Compound	⟨dist(8f–Fe)⟩ (Å)	⟨dist(8j–Fe)⟩ (Å)	⟨dist(8i–Fe)⟩ (Å)
$YFe_{11}Mo$	2.52	2.58	2.71
$YFe_{10}Mo_2$	2.52	2.60	2.73
$YFe_{9.5}Mo_{2.5}$	2.52	2.60	2.73
YFe_9Mo_3	2.53	2.61	2.75
$HoFe_{11}Mo$	2.50	2.58	2.71
$HoFe_{10}Mo_2$	2.51	2.59	2.72
$HoFe_{9.5}Mo_{2.5}$	2.52	2.59	2.72
$HoFe_9Mo_3$	2.52	2.60	2.75

Figures 2 and 3 illustrate the evolution of the cell parameters and of the cell volume with the Mo content. Published results on the Y compounds [5, 6] are also plotted in the figures, for comparison. It is seen that in the range of the studied Mo contents the variation of the cell parameters with the Mo content is in fact not linear, contradicting what is generally assumed. Extrapolating to $x = 0$ the a and c curves of the $YFe_{12-x}Mo_x$ series, the values $a = 8.48(5)$ Å and $c = 4.78(3)$ Å are obtained for YFe_{12}; these values are in good agreement with 8.478 Å and 4.762 Å extrapolated for YFe_{12} from the $YFe_{12-x}V_x$ series [9].

3.2. Magnetic behaviour

Figures 4 to 10 and table 3 present some selected magnetization results.

Figure 4 shows the thermal behaviour of the magnetization measured under a field of 5.0×10^{-3} T for Y and Ho compounds with $x = 2,3$. Zero-field cooled (ZFC) curves were recorded after cooling down the samples from 400 K to 10 K in zero applied field. Field cooled (FC) curves refer to the samples cooled under the measurement field. In both cases the measurements were performed with increasing temperature. All the studied samples present distinct ZFC and FC magnetization values. For the Y compounds the highest magnetization values in the FC curves are obtained at the lowest temperatures, corresponding to the orientation of the iron moments along the applied field. For the Ho series the highest magnetization value

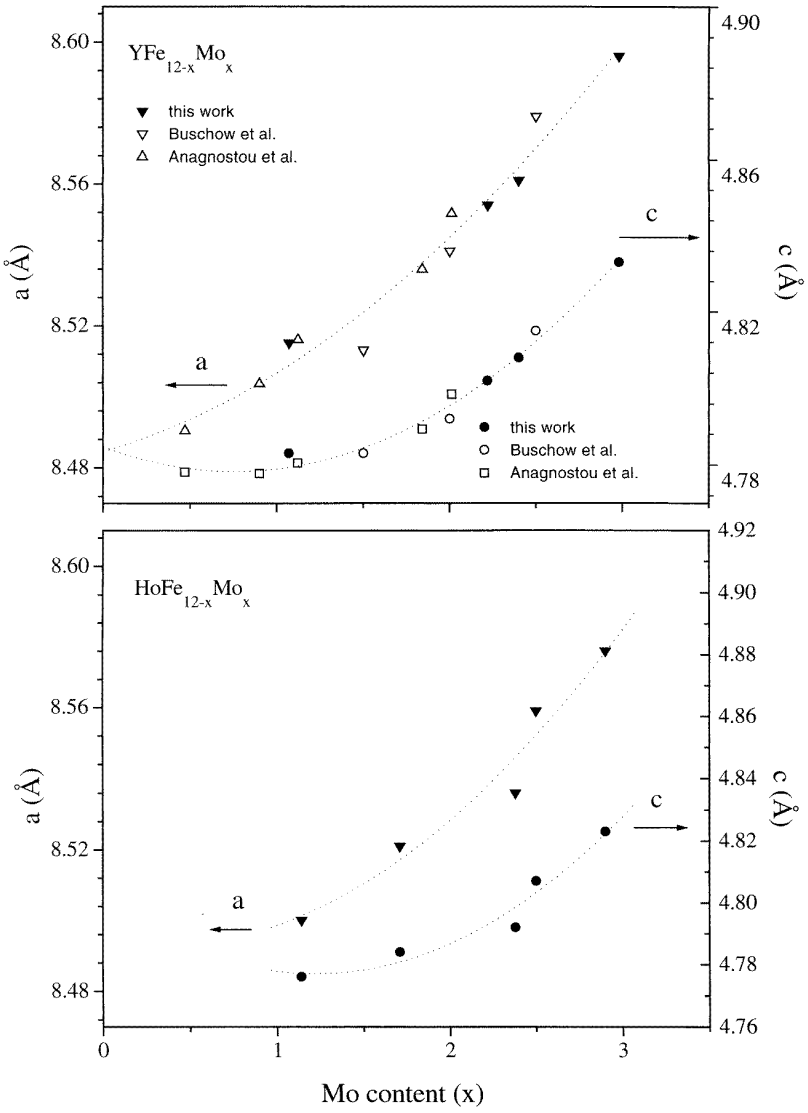

Figure 2. Lattice parameters a (solid triangles) and c (solid circles), refined from neutron diffraction patterns measured at room temperature and plotted as a function of the Mo concentration for Y and Ho samples. Some values found in the literature [5, 6] are presented for comparison (open symbols). The lines are guides to the eye.

in the FC curves is reached for temperatures around 100 K. This is related to the ferrimagnetic coupling between the rare-earth and the iron sublattices, which have different magnetization thermal behaviours. For x between 2 and 2.5 there is a compensation of the Ho and Fe sublattice moments, as the net magnetization changes sign (m_n in table 3).

Magnetization was measured as a function of the applied field up to 10 T for all samples. Figure 5 shows the results for the Ho samples. A ferromagnetic type behaviour with a superimposed linear dependence at higher fields is found, confirming the previous analysis. In the case of YFe_9Mo_3 (figure 6) there is a net decrease of the magnetization for temperatures

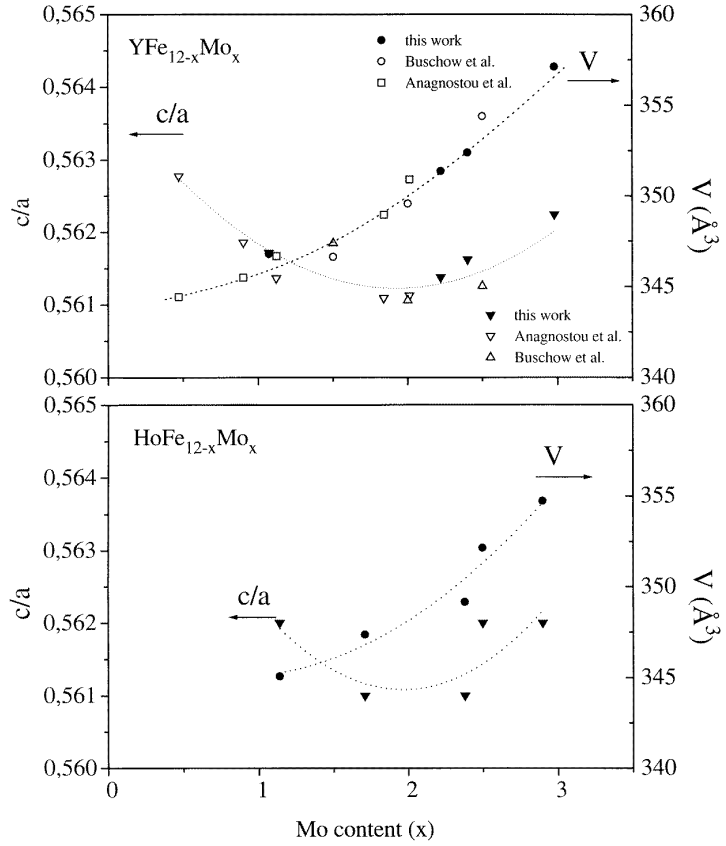

Figure 3. The c/a ratio (solid triangles) and unit cell volume, V (solid circles), refined from neutron diffraction patterns measured at room temperature and plotted as a function of the Mo concentration for Y and Ho samples. The lines are guides to the eye.

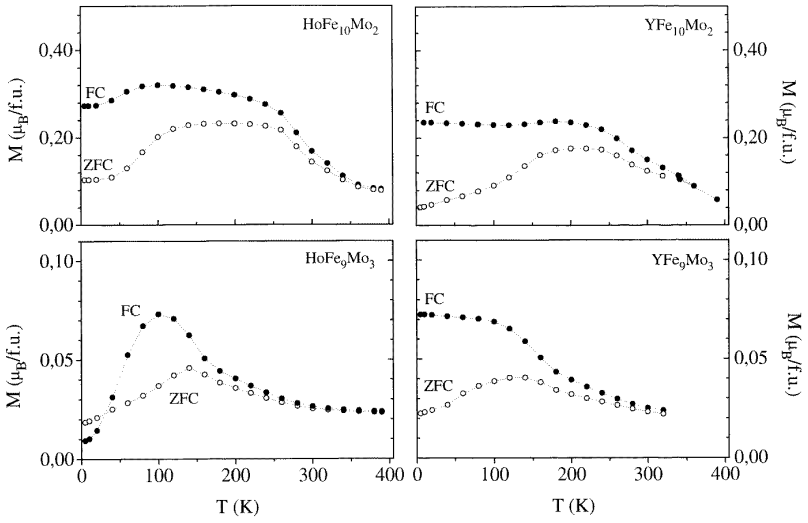

Figure 4. ZFC/FC (50 Oe) magnetization curves for the (Y, Ho)$Fe_{12-x}Mo_x$ ($x = 2, 3$) compounds.

Table 3. Magnetic characteristics at 6 K: μ is the magnetic moment, extracted from neutron diffraction analysis; m_n is the magnetic moment per formula unit calculated from neutron data; m_m is the magnetic moment per formula unit calculated from the spontaneous magnetization and T_C is the Curie temperature obtained from magnetization measurements.

Compound	Atom	μ (μB)	m_n (μ_B fu^{-1})	m_m (μ_B fu^{-1})	T_C (K)
	Y (2a)	—			
$YFe_{11}Mo$	Fe (8f)	2.0 (1)	23.0 (9)	19.6 (1)	470 (10)
	Fe (8i)	2.4 (1)			
	Fe (8j)	1.9 (1)			
	Y (2a)	—			
$YFe_{10}Mo_2$	Fe (8f)	1.6 (1)	17.4 (9)	12.6 (1)	295 (10)
	Fe (8i)	1.9 (3)			
	Fe (8j)	1.8 (1)			
	Y (2a)	—			
$YFe_{9.5}Mo_{2.5}$	Fe (8f)	0.9 (1)	9.5 (9)	8.5 (1)	290 (10)
	Fe (8i)	1.3 (3)			
	Fe (8j)	1.0 (1)			
	Y (2a)	—			
YFe_9Mo_3	Fe (8f)	—	—	1.8 (1)	140
	Fe (8i)	—			
	Fe (8j)	—			
	Ho (2a)	−10.0 (1)			
$HoFe_{11}Mo$	Fe (8f)	1.6 (1)	10.7 (9)	9.7 (1)	510 (10)
	Fe (8i)	2.1 (1)			
	Fe (8j)	2.0 (1)			
	Ho (2a)	−10.1 (1)			
$HoFe_{10}Mo_2$	Fe (8f)	1.2 (1)	2.9 (9)	3.7 (1)	280 (10)
	Fe (8i)	1.7 (2)			
	Fe (8j)	1.2 (1)			
	Ho (2a)	−9.1 (1)			
$HoFe_{9.5}Mo_{2.5}$	Fe (8f)	0.8 (1)	−0.7 (8)	1.4 (1)	230 (10)
	Fe (8i)	0.9 (2)			
	Fe (8j)	0.9 (1)			
	Ho (2a)	−6.4 (1)			
$HoFe_9Mo_3$	Fe (8f)	0.5 (1)	$\sim$ 0 (1)	2.0 (1)	170 (10)
	Fe (8i)	1.1 (1)			
	Fe (8j)	0.8 (1)			

lower than 20 K, only detectable in the $M(H)$ curves. The same behaviour was observed in $YFe_{9.5}Mo_{2.5}$ [10]. This loss of magnetization could be explained by a non-collinear distribution of the iron moment directions at low temperatures. In fact, Lorenz *et al* [11] have reported a calculation of the magnetic structure for $YFe_{12-x}Mo_x$ alloys, which predicts the existence of non-collinear Fe spin configurations. This analysis is based both on competing ferro- and antiferromagnetic exchange interactions related to variations of the Fe–Fe nearest neighbour distances with the Mo content, and a local spin anisotropy parametrized in terms of a spin–orbit contribution to the Hamiltonian interaction. However, our neutron diffraction experiments were not suitable for checking this Lorenz spin-resolved approach because only one measurement was performed, at 6 K.

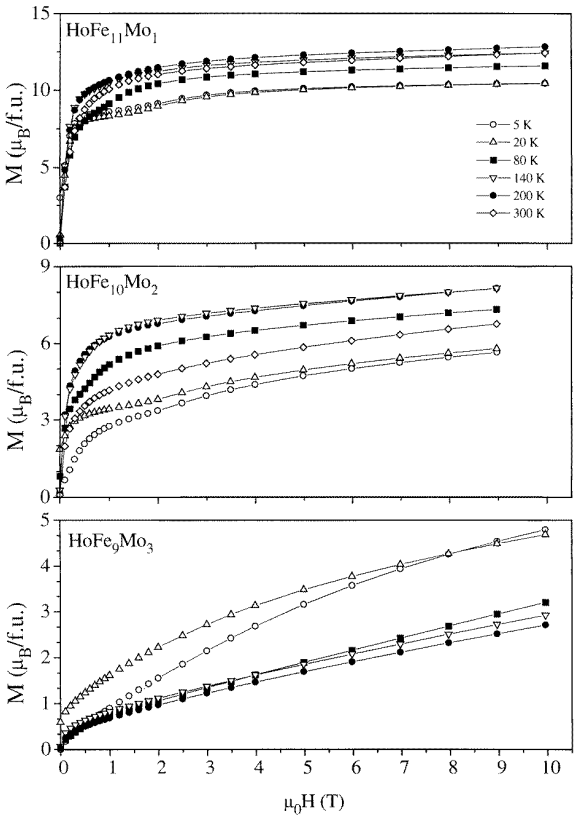

Figure 5. Magnetization measured as a function of the applied field for the Ho samples.

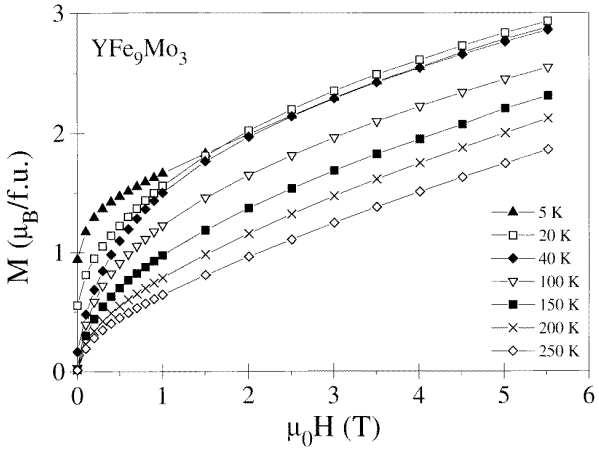

Figure 6. Magnetization measured as a function of the applied field for YFe_9Mo_3.

Figure 7 shows the magnetization of $HoFe_{11}Mo$ as a function of applied field for $T = 5$ K, both for H parallel and perpendicular to the c axis. The easy direction is the c axis, as

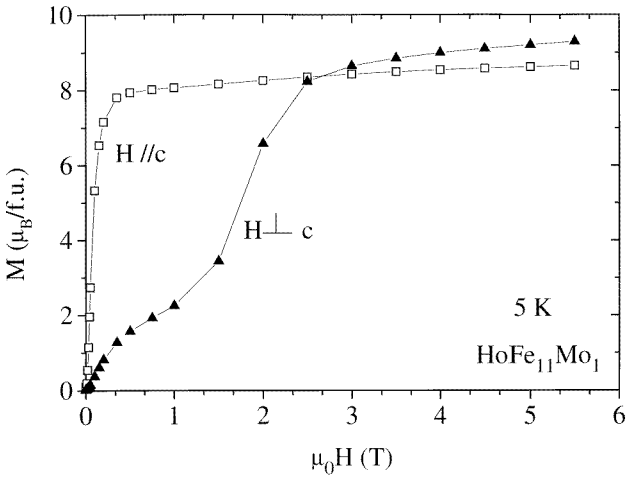

Figure 7. Magnetization curves of $HoFe_{11}Mo$ oriented sample.

expected from the well known easy axis contribution of the Fe sublattices and the dominant magnetocrystalline anisotropy term of the Ho site. For $H \perp c$ an anomaly is detected in the magnetization curve for fields around 1 T. This first order magnetization process (FOMP), also detectable in the non-oriented samples ($x = 1$ to 3) for the lowest temperatures, reveals an intermediate metastable magnetization state with a value of 2.5 μ_B fu^{-1}. The same kind of behaviour has been observed in other $RFe_{12-x}Mo_x$ compounds when R is magnetic [12], and has been attributed to a rotation of the magnetic moments under the external field.

From the magnetization curves (figure 7), using the saturation value for the easy axis direction, the anisotropy constant K_1 was determined. Based on the anisotropy energy $W_a = K_1 \sin^2\theta + K_2 \sin^4\theta + K_3 \sin^6\theta$, and assuming a small K_3 (10% K_1), the value of K_2 was fitted from the $M(H)$ curve for $H \perp c$. In figures 8(a) and (b) the total energy E (including anisotropy and Zeeman) is plotted as a function of the angle θ between the net magnetization and the c easy axis for different applied fields. The evolution of E with field shows that above 1.5 T the absolute minimum at $\theta = 16^\circ$ changes to a local minimum, explaining the marked increase in the net magnetization. From 1.5 to 2 T the magnetization rotates to about 50 degrees from the c axis. When the applied field is large enough to attain saturation ($H \leqslant 2.5$ T) the magnetization exceeds the values found for applied fields along the easy axis direction. This behaviour can be attributed to a field induced, non-collinear, arrangement of the Fe and Ho moments, with the Ho moments making an angle of about 67 degrees with the c axis, the Fe moments being almost forced into the basal plane.

In figures 9 and 10 the real part of the ac susceptibility is plotted as a function of temperature for the different samples, showing a clear maximum in all cases. In general, for $x > 2$ the temperatures associated with these maxima are different from the T_C values obtained by magnetization. This is due to the fact that magnetization results are the average of the magnetic moment contributions, while ac magnetic susceptibility is sensitive to the dynamic behaviour of the magnetic moments. Similar differences in the T_C values were observed in $RFe_{9.5}Mo_{2.5}$ systems [13]. In that study, the Mössbauer spectroscopy results evidenced distinct magnetic behaviours for the three Fe sites, resulting in broad order/disorder transitions. The ac susceptibility maxima become broader for compounds with $x > 2$, corresponding to a broader distribution of the ordering temperatures, as can be seen in figures 9 and 10. The ordering

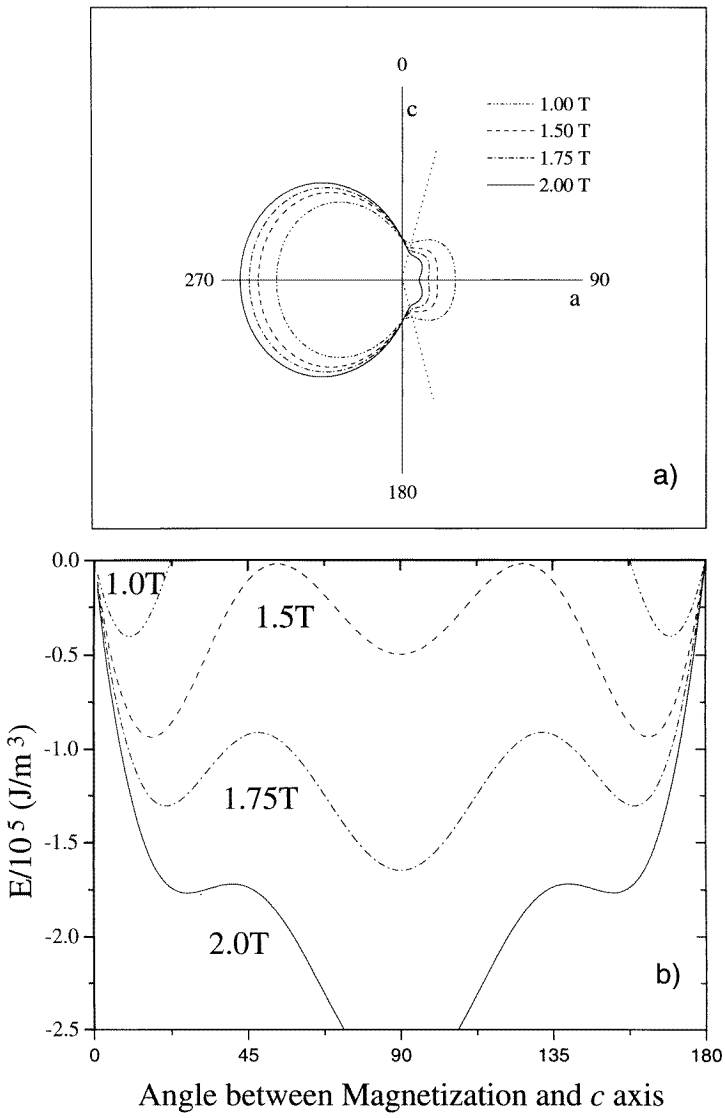

Figure 8. (*a*) Polar representation of the total energy (anisotropy + Zeeman) calculated for $HoFe_{11}Mo$ for different applied field intensities. (*b*) Total energy represented as a function of the angle between the net magnetization and the *c* easy axis, for angles between 0° and 180°. This is part of the diagram plotted in (*a*).

temperatures obtained from the inflection points in the FC curves and from ac susceptibility results for the samples with $x = 1$ are presented in table 3.

Also in the same table, the spontaneous magnetization values (m_m), obtained by extrapolation to $H = 0$ of the higher field behaviour of the magnetization isotherms recorded at 5 K, are reported. The difference between these values and the m_n values obtained by neutron diffraction can be attributed to the negative magnetic contribution of the conduction electrons. This component, that can not be detected by neutron diffraction, may be associated with the negative exchange coupling between the 3d electrons and the conduction electrons [14, 15].

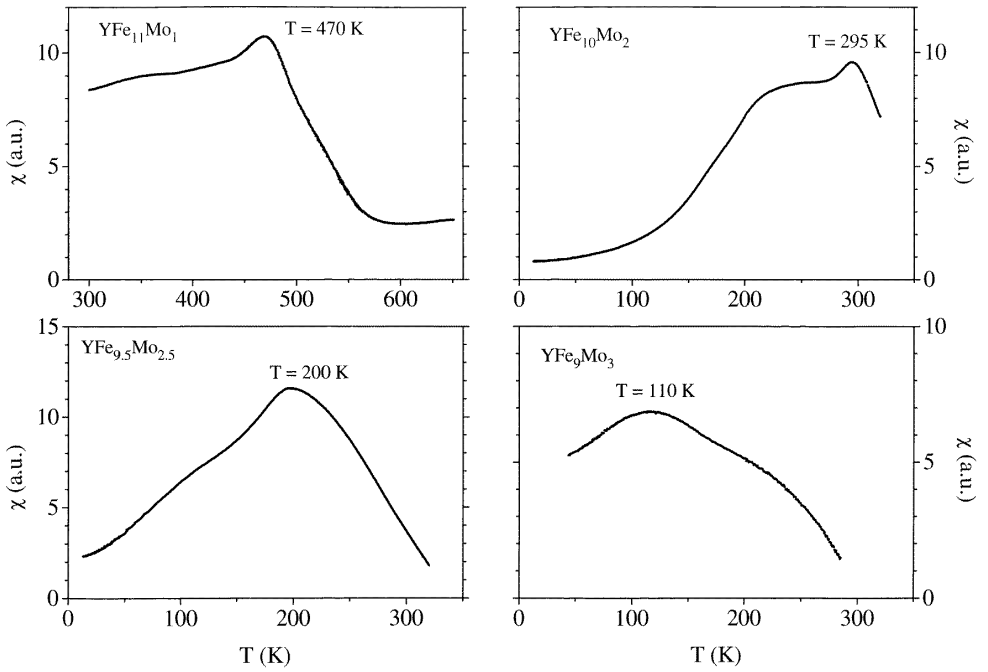

Figure 9. Temperature dependence of the real part of the ac susceptibility of the $YFe_{12-x}Mo_x$ compounds.

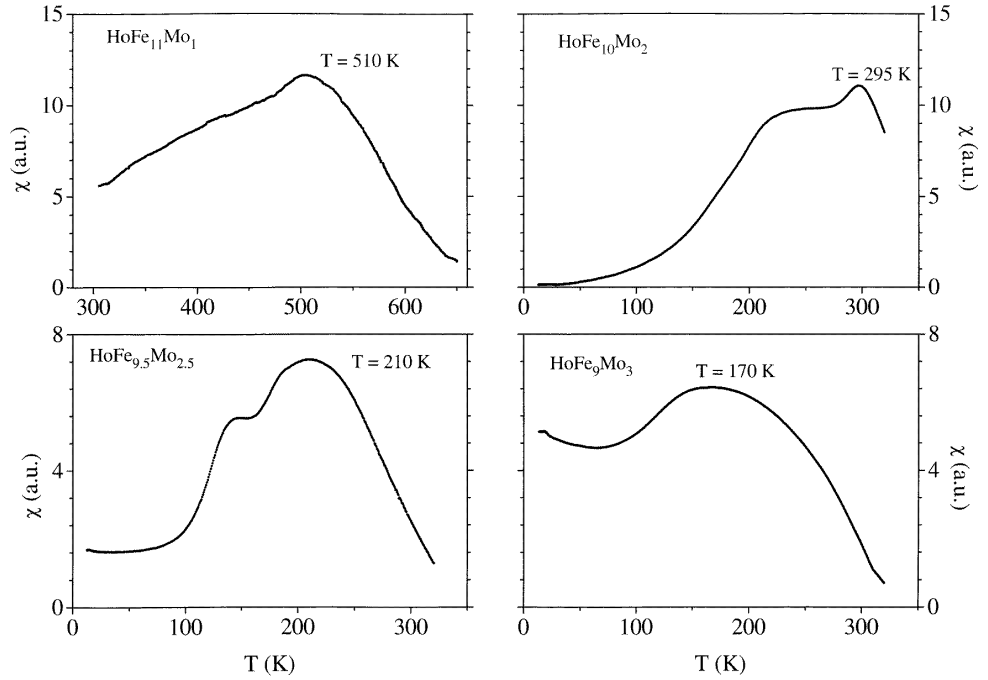

Figure 10. Temperature dependence of the real part of the ac susceptibility of the $HoFe_{12-x}Mo_x$ compounds.

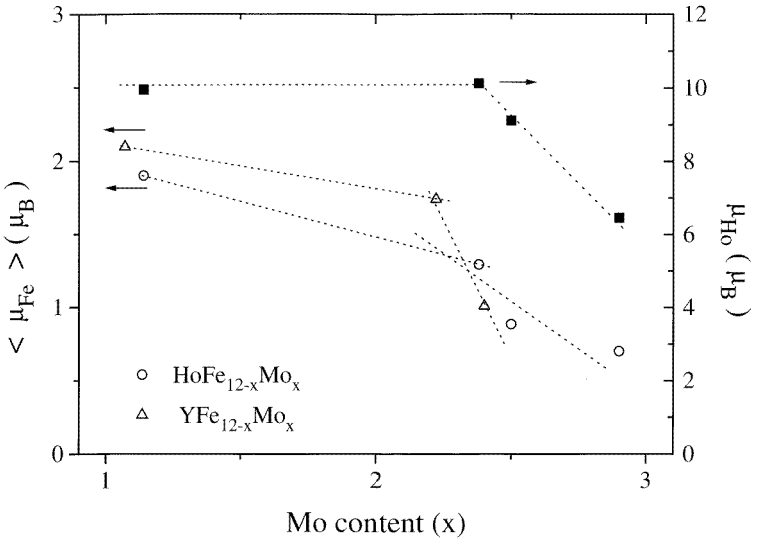

Figure 11. The average iron moments at 6 K, plotted as a function of the Mo concentration for the Y and Ho series. Also plotted are the Ho moments for the Ho series.

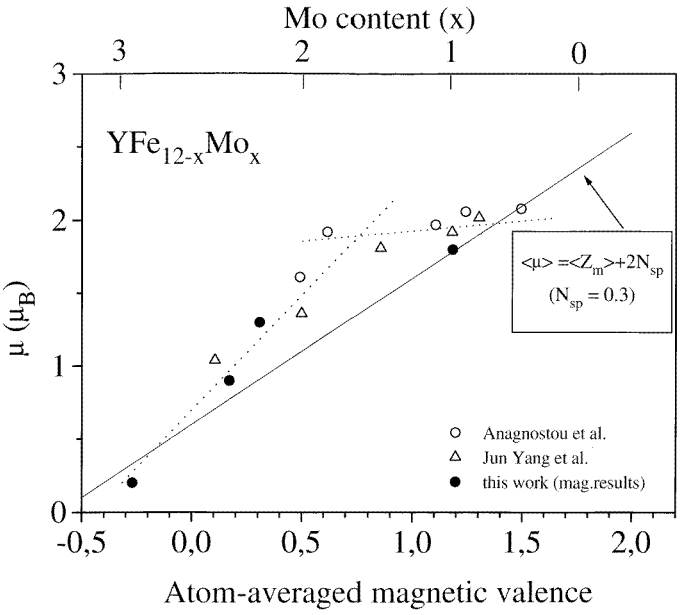

Figure 12. Magnetization per iron atom versus average magnetic valence. The solid line is the generalized Slater–Pauling curve.

The R and Fe magnetic moments deduced from the neutron analysis at 6 K are presented in table 3. For all samples in both series the relation between the different iron moments is $\mu(8i) \geqslant \mu(8j) \geqslant \mu(8f)$, following the trend of the Wigner–Seitz cell volumes for the three iron sites [16].

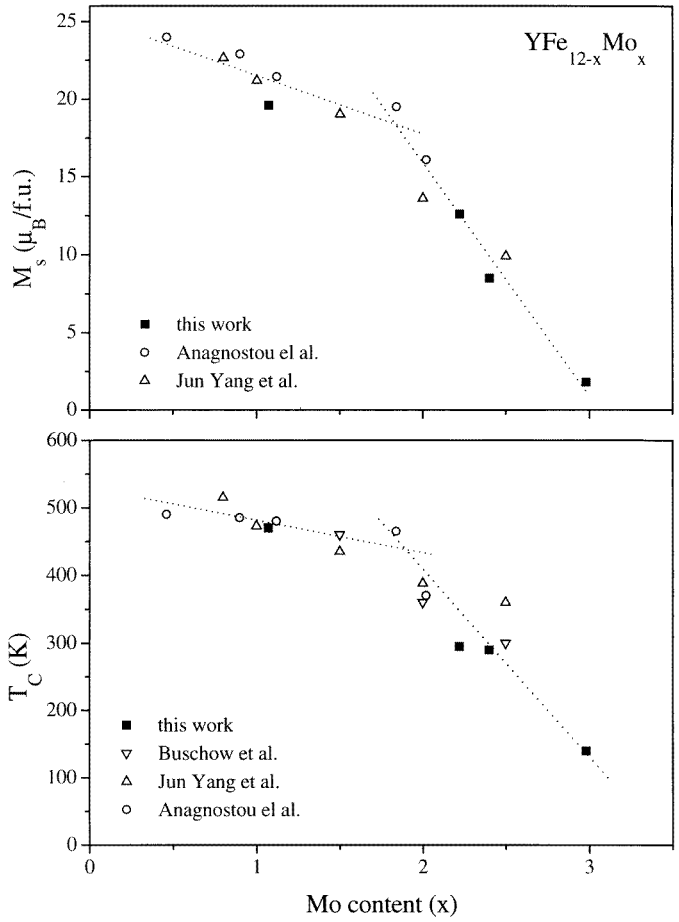

Figure 13. Curie temperature and spontaneous magnetization plotted as a function of the Mo concentration for the Ho and Y series.

The average iron magnetic moments at 6 K for the Y and Ho series are plotted in figure 11, as a function of the Mo concentration. The corresponding Ho magnetic moment is also shown in the same figure. In Y samples with low Mo content, the variation is consistent with the results obtained from electronic structure calculations [8, 17] and photoemission data for Y series [18]. These results show that the average iron moment decreases due to the increasing Mo contribution to the d states near the Fermi level, giving rise to a strong hybridization of the Fe and Mo d bands. Above $x = 2$ a net reduction in the magnetic moments can be observed. For $HoFe_9Mo_3$ the Ho moment is 50% lower than the theoretical value and for YFe_9Mo_3 no magnetic contribution to diffraction is observed, meaning that the magnetic moments are smaller than 0.3 μ_B. This behaviour is most certainly related to a much stronger overlap between the non-magnetic Mo bands and the 3d Fe band. This is consistent with the fact, already pointed out in section 3.1, that the increase in Mo content is not followed by a subsequent cell expansion, in spite of the larger size of the Mo atoms.

The observed behaviour in the variation of the magnetic moment with Mo concentration does not agree with the linear variation expected from the generalized Slater–Pauling curve

[19, 20]. According to this model the average iron magnetic moment varies linearly with the magnetic valence, $Z_m = 2N_d\uparrow - Z$, where $N_d\uparrow$ is the contribution of the d band to the number of valence electrons with spin up and Z is the chemical valence. Figure 12 shows the magnetization per iron atom as a function of the average magnetic valence. It also shows the predicted generalized Slater–Pauling curve $\langle\mu\rangle = \langle Z_m\rangle + 2N_{sp}$, where N_{sp} is the contribution of the s–p bands to the number of valence electrons close to 0.3 atoms/spin [19]. Clearly for $YFe_{12-x}Mo_x$, the consequence of the Fe–Mo substitution in the average moment can be described by two regimes with a crossover around $x = 2$. This value corresponds also to critical changes in the structural properties mentioned above (figure 3). Very significantly we find the same presence of two regimes in the evolution of T_C and M_S with the Mo content, as shown in figure 13 where results obtained by other authors were also included [5, 6].

4. Conclusions

Mo substitution for iron was studied in $RFe_{12-x}Mo_x$ (R = Y, Ho) compounds and a strong effect both on structural and magnetic properties was detected. A non-linear dependence of cell parameters, magnetic moments, spontaneous magnetization and order/disorder transitions with Mo increase was observed for both series. The results obtained, together with previously published data, clearly show the existence of a critical Mo concentration for $x \approx 2$. This unexpected behaviour is observed both in the structural and magnetic results and is interpreted as being due to the strong overlap between the non-magnetic Mo bands and the 3d Fe band, occurring above that Mo concentration. Although no simple correlation can be established between both types of property, a band structure calculation will certainly contribute to understanding the correlation between the dramatic drops of T_C and M_s (not supported by the magnetic valence model) and the change in the crystal structure induced by molybdenum substitution.

Acknowledgments

This study was partly funded by the Portuguese-French JNICT-CNRS collaboration and by the EEC-HCM scheme of grants.

References

[1] Li H S and Coey J M D 1991 *Handbook of Magnetic Materials* vol 6, ed K H J Buschow (Amsterdam: North-Holland) p 3
[2] Florio J V, Rundle R E and Snow A I 1952 *Acta Crystallogr.* **5** 449
[3] Helmholdt R B, Vleggaar J J M and Buschow K H J 1988 *J. Less-Common Met.* **138** L11
[4] Denissen C J M, Coehoorn R and Buschow K H J 1990 *J. Magn. Magn. Mater.* **87** 51
[5] Buschow K H J and Mooij D B 1989 *Concerted European Action on Magnets (CEAM)* ed I V Mitchell, J M D Coey, D Givord, I R Harris and R Hanitsch (London: Elsevier) p 63
[6] Anagnostou M, Devlin E, Psycharis V, Kostikas A and Niarchos D 1994 *J. Magn. Magn. Mater.* **131** 157
[7] Rodriguez-Carvajal J 1990 *Abstracts Satellite Meeting 15th Congress IUCr (Toulouse, 1990)* p 127
[8] Ishida S, Asano S and Fujii S 1994 *Physica* B **193** 66
[9] Verhoef R, de Boer F R, Zhi-Dong Zhang and Buschow K H J 1988 *J. Magn. Magn. Mater.* **75** 319
[10] Ayres de Campos J, Ferreira L P, Godinho M, Gil J M, Mendes P J, Ayres de Campos N, Ferreira I C, Bououdina M, Bacmann M, Soubeyroux J-L, Fruchart D and Collomb A 1998 *J. Phys.: Condens. Matter* **10** 4101
[11] Lorenz R, Hafner J, Jaswal S S and Sellmyer D J 1995 *Phys. Rev. Lett.* **74** 18 3688
[12] Kou X C, Sinnecker E H C P, Grossinger R, Wiesinger G, Zhao T, Liu J P and de Boer F R 1995 *J. Magn. Magn. Mater.* **140–144** 1025

[13] Ayres de Campos J, Gil J M, Mendes P J, Ferreira L P, Ferreira I C, Ayres de Campos N, Estrela P, Godinho M, Bououdina M, Collomb A, Fruchart D, Soubeyroux J-L, Takele S, Pelloth J and Brand R A 1996 *J. Magn. Magn. Mater.* **164** 305
[14] Mook H A and Shull C G 1966 *J. Appl. Phys.* **37** 1034
[15] Franse J M M and Radwansky R J 1999 *Supermagnets, Hard Magnetic Materials* eds G J Lang and F Grandjean (Dordrecht: Kluwer) p 119
[16] Isnard O and Fruchart D 1994 *J. Alloys Compounds* **205** 1
[17] Al-Omari I A, Jaswal S S, Fernando A S and Sellmyer D J 1994 *Phys. Rev.* B **50** 12 665
[18] Fernando A S, Woods J P, Jaswal S S, Welipitiya D, Patterson B M and Sellmeyer D J 1994 *J. Appl. Phys.* **75** 6303
[19] Williams A R, Moruzzi V L, Malozemoff A P and Terakura K 1983 *IEEE Trans. Magn.* **MAG-19** 1983
[20] Malozemoff A P, Williams A R and Moruzzi V L 1984 *Phys. Rev.* B **29** 1620